Materials Today Sustainability 26 (2024) 100792

Contents lists available at ScienceDirect

Materials Today Sustainability

journal homepage: www.journals.elsevier.com/materials-today-sustainability

Matrix curing and stress field development around fiber during the solvent evaporation-induced repolymerization of recycling composites

Christopher Chung, Huan Jiang, Chaoqian Luo, Kai Yu *

Department of Mechanical Engineering, University of Colorado Denver, Denver, CO, 80217, USA

ARTICLE INFO

Keywords:
Bond exchange reactions
Solvent evaporation
Network repolymerization
Diffusion-reaction-mechanics
Composite recycling

ABSTRACT

When recycling fiber-reinforced composites using depolymerized polymer solutions, oligomers reconnect through covalent bond exchange reactions (BERs), which ultimately forms a crosslinked network with mechanical properties comparable to those of virgin materials. This process offers exciting opportunities for the primary recycling of engineering composites, but it is intricately influenced by a few material and process parameters, such as heating temperature, duration, and fiber volume fractions. These parameters collectively determine the matrix's curing degree and the evolution of stress fields around the fiber, which are significant factors determining the quality and mechanical performance of recycled composites. This study introduces a diffusion-reaction-mechanics finite-element computational model to examine the solvent-induced repolymerization process in recycling composites. The model predicts the matrix curing degree, residual stress development around the fiber, and the composite's mechanical properties, aligning with experimental results. Parametric computational studies are then conducted to assess the influences of temperature, fiber content, solvent diffusivity, and the reactivity of BERs. The objective is to identify material and processing conditions that ensure efficient composite recycling while minimizing the development of residual stress. Overall, this study enhances our understanding of the mechanisms behind composite recycling using organic solvents and provides valuable insights for industrial stakeholders looking to optimize processing conditions and advance the commercialization and widespread adoption of this innovative recycling technique.

1. Introduction

Thermosetting composites offer a unique combination of characteristics, including high strength, lightweight, thermal stability, and resistance to chemicals [1]. They have found widespread application in high-performance sectors such as automotive, construction, and sports engineering [2,3]. However, recovering valuable resources and carbon fiber from composite scraps poses grand challenges due to the crosslinked nature of the polymer matrix [4], which cannot flow upon heating and thus cannot be reprocessed and recycled. As the utilization of thermoset composites continues to rise, the accumulation of their waste materials has reached a significant and concerning level.

Existing mechanical [5–10], thermal, or chemical treatments [11–19] for composite waste, such as pyrolysis, solvolysis, or fluidized bed processes, have demonstrated the capability to decompose the thermoset matrix and recover embedded carbon fibers, but they typically demand harsh processing conditions of high temperature, pressure, and supercritical acid, which raise environmental concerns and pose economic challenges. For instance, in a standard pyrolysis procedure, the operating temperature often falls within the range of 400–700 °C depending on the composition of the composite waste. Furthermore, after the polymer matrix is completely decomposed, the resulting product comprises a complex mixture of gaseous, liquid, and solid chemicals. These byproducts are difficult to purify and reuse, potentially leading to the generation of secondary waste streams.

In recent years, innovative recycling methods based on solvent-assisted selective cleavage of chemical bonds have emerged [20–39]. The concept involves submerging composite scraps in an appropriate organic solvent at elevated temperatures. As solvent molecules diffuse into the matrix network, they react with specific covalent bonds on the polymer chain backbone, leading to the cleavage of polymer chains. This process ultimately results in the depolymerization of the polymer matrix into soluble oligomers, allowing for the recovery of clean fibers. As notable examples, ester bonds are found in a wide variety of thermosetting polymers. Yu et al. [35] have demonstrated that such thermosets can be fully depolymerized using an alcohol solvent mixed with a

* Corresponding author.
E-mail address: kai.2.yu@ucdenver.edu (K. Yu).

https://doi.org/10.1016/j.mtsust.2024.100792
Received 7 November 2023; Received in revised form 25 March 2024; Accepted 28 April 2024
Available online 30 April 2024

catalyst for transesterification. In comparison to traditional thermal and chemical waste treatments, solvent-assisted depolymerization typically employs mild processing temperatures and low-toxicity solvents, promoting a green and sustainable approach to waste reprocessing. Furthermore, the depolymerization process can be reversible. By heating the depolymerized polymer solution in an open environment to encourage solvent evaporation, the network can be repolymerized with a nearly identical microscale network structure and mechanical strength [40–43]. This solvent evaporation-induced repolymerization process can be harnessed to create new composites using reclaimed feedstock resins, as illustrated in Fig. 1.

The repolymerization process of the polymeric matrix plays a significant role in determining the quality of recycled composites. It involves complex interactions among several factors, including the diffusion of reactive solvent, dynamic bond exchange reactions (BERs), and the evolution of stress fields. These interactions are further influenced by the content and arrangement of embedded carbon fibers. Firstly, since solvent evaporation drives the network's repolymerization, the outer layers solidify rapidly, impeding solvent transport and the curing of polymeric materials beneath them. This non-uniform solvent content, functional group conversion, and network structure development result in thickness-direction inhomogeneities. Using a lower processing temperature can mitigate the formation of non-uniform material properties, but the tradeoff is the reduced repolymerization speed. Additionally, the presence of carbon fibers within the composite system blocks the transportation of solvent molecules and thus reduces the overall recycling speed.

Secondly, if the precursor polymer solution contains a substantial amount of unreacted solvent, the repolymerization process leads to noticeable volume shrinkage and the development of residual stresses within the polymer matrix. These significant stress concentrations around the fibers can cause delamination between the fiber and matrix, as well as at the fiber-polymer interface. This, in turn, can result in potential void formation at the fiber/matrix interface, fiber misalignment, and distortion of the fabricated composite structures.

The intricate interactions during the repolymerization of thermoset composites impose challenges in identifying the optimal processing conditions for recycling. There is a pressing need for fundamental research to reveal the material-process-property relationships, which are essential for the production of high-quality recycled composites. It is also critical for industrial sectors looking to comprehend the recycling process and develop economically viable business models for large-scale engineering applications. However, to the best of our knowledge, there is no prior work that addresses the coupled diffusion, reaction, and mechanical aspects inherent to the solvent evaporation-induced repolymerization process in recycling composites.

In this paper, a finite element analysis (FEA) computational model is defined to study the repolymerization process of thermoset composites. An epoxy-based thermosetting polymer with transesterification-type BERs [44–47] is used as the material platform. The influences of heating temperature on the residual stress development and the non-uniform material properties along the thickness direction are investigated. The computational model is shown to closely capture the experimental data. It is then employed to perform parametric studies to reveal the influences of fiber content on the recycling rate of composites, as well as the development of residual stress around the embedded fibers. The influences of solvent diffusivity and reactivity of transesterification are also presented. The study revealed influencing mechanisms of various material and processing conditions, as well as the optimal processing to enable high-quality recycled thermoset composites. This research paves the way for the broader adoption of solvent-assisted recycling techniques in addressing the issue of composite waste reduction.

2. Materials and experimental methods

2.1. Preparation of depolymerized polymer solution

The repolymerization process started with a fully depolymerized epoxy solution. The epoxy materials used were the epoxy-based thermoset developed by Leibler and coworkers [44]. This thermoset was synthesized using the crosslinker fatty acids (Pripol 1040, Croda, Houston, TX), the epoxy monomer bisphenol A diglycidyl ether (DGEBA, Sigma Aldrich, St. Louis, MO), and the catalyst triazabicyclodecene (TBD) for transesterifications (Sigma Aldrich). The detailed chemical structures of reactive monomers, catalyst, and the synthesized epoxy network are presented in the Supplementary Material (Section S1).

As shown in Fig. 1a, the epoxy scraps were first immersed in ethylene glycol (EG) solvent at 180 °C for network depolymerization. An excessive amount of solvent was used to ensure complete depolymerization of the network into soluble chain segments. The volume ratio between the polymer and solvent was 1:3. During the heating, the container was sealed to prevent solvent evaporation. Once the sample had fully depolymerized, the quantity of unreacted solvent molecules was determined, taking into account that the amount of reacted EG molecules equaled the amount of ester bonds present within the epoxy network.

To mitigate significant volume shrinkage during the subsequent repolymerization process, the polymer solution was further heated at 180 °C in an open environment. During this process, the mass reduction in the system primarily resulted from the evaporation of unreacted EG solvents. We closely monitored the weight of the mixture to ensure that the amount of unreacted EG solvent was negligible, and the system mainly contained cleaved polymer chains.

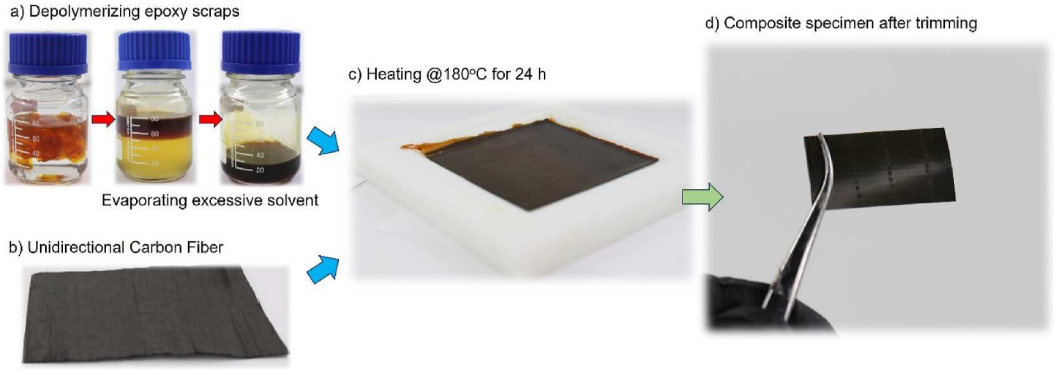

Fig. 1. Fabrication of composites through solvent-evaporation induced epoxy repolymerization. (a) Depolymerizing ester-containing epoxy scraps in the 180 °C ethylene glycol solvent followed by evaporating excessive solvent. (b) Uniaxial carbon fiber fabric used as the reinforcing material. (c) Molding the epoxy solution with the fiber fabric, where the epoxy matrix gradually repolymerizes as the solvent evaporates from the top surface. (d) A finished composite sample after trimming.

2.2. Characterizations of epoxy during the repolymerization

The properties of pure epoxy during the repolymerization process were first characterized, including weight changes, volume shrinkage, residual stress, solvent diffusivity, and elastic modulus. All these parameters have been thoroughly tested in our previous studies using the same materials [48–50]. We briefly describe the experimental procedure here. Detailed experimental descriptions are presented in the Supplementary Material (Section S2).

The rate of weight loss and solvent evaporation was determined by monitoring the sample's weight over time during the heating process. To determine the network volume shrinkage degree, the polymer solution was first heated until it reached the gelation point and could carry the load. It was then subjected to testing using Dynamic Mechanical Analysis (DMA, TA Instruments, New Castle, DE) at constant temperatures (160 °C, 180 °C, and 200 °C, respectively). When no force was applied, the sample was heated in a free-standing state, with the resulting volume change being recorded as a function of time. On the other hand, when the sample was fixed during the isothermal heating process, the stress accumulation within the network due to volume shrinkage was recorded.

Solvent diffusivity within epoxy networks with varying degrees of curing was determined using the standard swelling tests in the EG solvent. The elastic modulus of the thin-film epoxy sample was determined through room-temperature uniaxial tension tests. To characterize the non-uniform material properties during the repolymerization of bulk epoxy, the polymer solution was poured into a mold. Subsequently, after heating for a given duration, the sample was extracted and sectioned into layers parallel to the thickness direction of the specimen. Each layer's thickness was approximately 1.5 mm. These sliced samples were then subjected to DMA tests to evaluate their average elastic modulus.

2.3. Characterizations of epoxy composites during the repolymerization

Composite lamina samples were fabricated using the depolymerized polymer solution. The solution was poured into a mold with a unidirectional fiber layer securely in the middle, with a fiber volume fraction of 37%. The mixture was then heated in an oven at 180 °C and 200 °C, respectively. The modulus of the composite lamina during repolymerization was characterized in the transverse direction of carbon fiber to determine the influences of matrix curing. Periodically, the transverse modulus (within the first 1% strain) was measured using uniaxial tension tests at room temperature.

3. Computational modeling

3.1. Overview of the modeling framework

The overall computational modeling framework of the composite repolymerization is shown in Fig. 2. In this study, the length of the composite lamina samples is significantly larger than the average cross-section size. When these composite samples are subjected to heating in an open environment, the repolymerization process mainly occurs on the top and bottom surfaces, while the reaction along the length direction is less pronounced due to the smaller evaporation area. Consequently, the repolymerization process is taken to be a 2D plane-strain diffusion-reaction-mechanics problem.

Within the modeling framework, individual fibers are assumed to be unreactive with solvent molecules, and their positions are fixed in space. For a fully depolymerized solution, the system is initially in an equilibrium state. By applying a solvent evaporation boundary condition to the top surface, it prompts diffusion of solvent molecules in the vertical direction of the system, and the equilibrium of reversible reactions shifts toward chain connection. From the bottom to the surface, the solvent content gradually decreases, and the matrix degree of curing gradually increases.

3.2. Continuum-level modeling

3.2.1. Stress-strain relationships

Since the modulus of the embedded carbon fiber is significantly higher than that of the epoxy matrix, and they do not react with the solvent, the carbon fiber is modeled as a rigid solid within the FEA model. For the matrix material, the total deformation gradient $\boldsymbol{F}$ can be

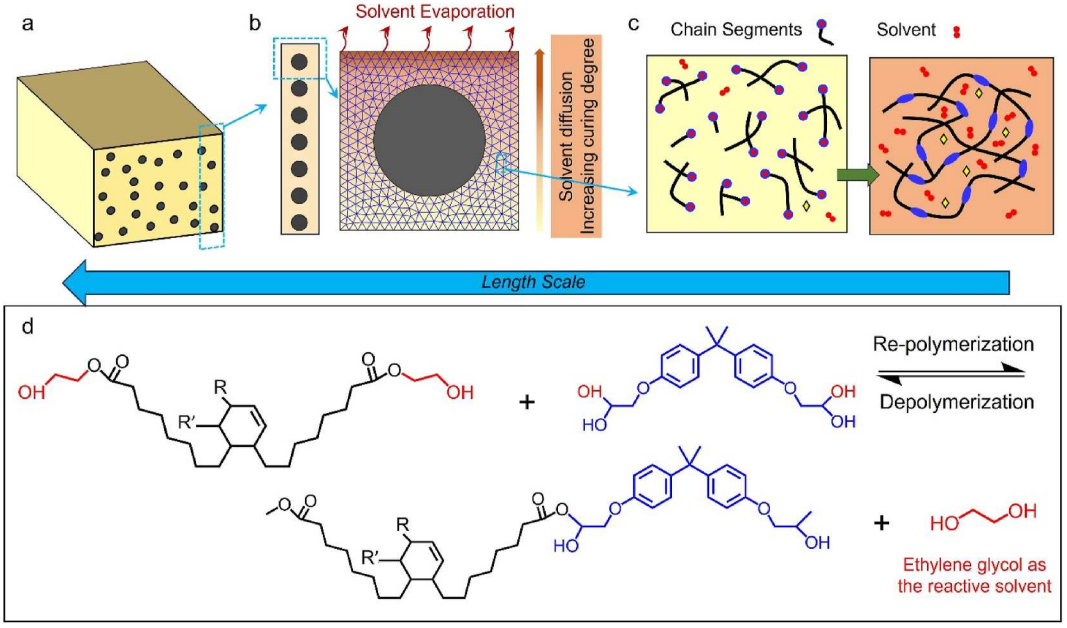

Fig. 2. Overall modeling framework and the repolymerization mechanism of the matrix epoxy. (a) Schematic representation of a macroscopic composite lamina sample with continuous carbon fiber reinforcement. (b) A reduced-size representative FEA model to study the repolymerization process with a solvent-evaporation boundary condition applied to the top surface. (c) A schematic view of the network repolymerization. (d) The microscale transesterifications of chain segments lead to chain connection.

decomposed as [51–53]:

$$\boldsymbol{F} = \boldsymbol{F}_M \boldsymbol{F}_V \tag{1}$$

where $\boldsymbol{F}_M$ is the mechanical deformation gradient and gives rise to stresses. $\boldsymbol{F}_V$ is the volume change of the matrix material due to the solvent evaporation and network polymerization.

Since the BERs effectively release the internal stress following an exponential function [47], the mechanical deformation gradient is further decomposed into an elastic and viscous part as a Maxwell element, namely $\boldsymbol{F}_M = \boldsymbol{F}_e \boldsymbol{F}_v$. The Cauchy stress is:

$$\boldsymbol{\sigma}(\boldsymbol{x},t) = \frac{E(\boldsymbol{x},t)}{3}\boldsymbol{F}_e \boldsymbol{F}_e{}^T - p\boldsymbol{I} \tag{2a}$$

where p is a fitting parameter determined by the mechanical boundary condition. The elastic modulus is a function of network curing degree. According to the previous work [48], it scales to the network degree of curing as:

$$E(\boldsymbol{x},t) = E_\infty P^{6\alpha}(\boldsymbol{x},t) \tag{2b}$$

where α is a correlation exponent, and E_∞ is the modulus of a fully cured network. P is the degree of curing (varies from 0 to 100%) of the repolymerizing network, which depends on the reaction kinetics and will be introduced in detail in the following section.

On the other hand, during the repolymerization, the average length of chain segments gradually increases, which influences the relaxation time. According to the principles of polymer physics [54], the relaxation time for an entangled polymer melt scales with the number of Kuhn segments N (or the length of chain segments) as $\tau_M \sim N^2$. Given these considerations, we propose the following relationship:

$$\tau_M = \xi \left[\frac{N_{ave}(t)}{N_\infty}\right]^2 (k_2 N_A)^{-1} \tag{3}$$

where ξ is a fitting parameter to be determined from experiment. N_∞ is the chain segment length of fully cured epoxy network. N_{ave} is the current average chain segment length. Detailed expressions of chain connection and cleavage rates, k_1 and k_2, will be addressed in the subsequent section using microscale statistical analysis.

3.2.2. Solvent transportation

At a given material point with position $\boldsymbol{x}(x_1, x_2, x_3)$, the transportation of solvent within the system is assumed to adhere to Fick's second law. The mole concentration of solvent molecules, denoted as $C_s(\boldsymbol{x},t)$, can be described as follows:

$$\frac{\partial C_s(\boldsymbol{x},t)}{\partial t} = D_s(\boldsymbol{x},t)\frac{\partial^2 C_s(\boldsymbol{x},t)}{\partial x^2} + k_s(\boldsymbol{x},t) \tag{4a}$$

where D_s denotes the solvent diffusivity, and k_s denotes the changing rate due to the transesterification BERs. Both parameters depend on the network curing degree, and thus are functions of position $\boldsymbol{x}(x_1, x_2, x_3)$ and heating time t.

The temperature dependence of D_s follows the Arrhenius law. According to Krongauz et al. [55], the solvent diffusivity is scaled with the network curing degree, P, by an exponential relationship. With these considerations, the D_s is formulated as:

$$D_s(\boldsymbol{x},t) = \underbrace{D_{s0}}_{\substack{\text{Reference}\\ \text{Diffusivity}}} \underbrace{\exp\{\beta[1-P(\boldsymbol{x},t)]\}}_{\substack{\text{Repolymerization Curing}\\ \text{Degree}}} \underbrace{\exp\left[-\frac{E_s}{R(T+273)}\right]}_{\text{Temperature}} \tag{4b}$$

In the above equation, D_{s0} represents the reference diffusivity at 140 °C, E_s being the energy barrier, and R being the gas constant. β is a fitting parameter determined from experiment.

3.2.3. Solvent evaporation

The solvent evaporates on the surface of the sample. The solvent evaporation flux, J_e (mol/m^2s), on the polymer-air interface is defined as:

$$J_e(\boldsymbol{x},t) = K_s C_s(\boldsymbol{x},t) \tag{5a}$$

where K_s (m/s) is the mass transfer coefficient, which depends on the repolymerization temperature as:

$$K_s(T) = K_{s0}\exp\left[-\frac{E_k}{R(T+273)}\right] \tag{5b}$$

where K_{s0} is the reference mass transfer coefficient, and E_k is an energy term related to the temperature influences. They are both determined through calibrating with the experimental data.

3.2.4. Network volume shrinkage

The network volume shrinkage during the repolymerization is assumed to be isotropic, i.e.,

$$\boldsymbol{F}_V = \delta_v \boldsymbol{I} \tag{6a}$$

As the solvent evaporates and the network repolymerization proceeds, the volume shrinkage occurs due to the loss of solvent molecules and network polymerization. In this study, we assume that these two processes are uncoupled when determining volume shrinkage. The changing rate of the volume shrinkage strain can be expressed as follows:

$$\dot{\delta}_v(\boldsymbol{x},t) = w_1 \dot{C}_s(\boldsymbol{x},t) M_s/\rho_s + w_2 \dot{P}(\boldsymbol{x},t) \tag{6b}$$

where w_1 and w_2 are weight coefficients. M_s is the solvent molecular weight, ρ_s is the solvent density.

3.3. Microscale reaction kinetics and degree of curing

The network curing degree, $P(\boldsymbol{x},t)$, is determined by considering the microscale reactions of chain cleavage and connection. It is noted that the solvent plays two roles in the re-polymerization process. Firstly, it acts as a reaction medium. Its evaporation induces a concentration gradient of monomers, thus affecting the reaction kinetics. Secondly, the solvent molecules participate in the reactions themselves. As depicted in Fig. 2d, when the monomers connect with each other during the re-polymerization reaction, solvent molecules are generated within the system. Without the evaporation of the solvent, the system remains in a dynamic equilibrium condition, and the degree of curing within the network will not increase. It is only after the solvent molecules evaporate out of the system that the equilibrium shifts towards re-polymerization.

At a specific position, $\boldsymbol{x}$, the rates of chain connection (k_1) and cleavage (k_2) during the re-polymerization are formulated based on the diffusivity of solvent molecules and chain segments as well as their contents and average distance. For the chain connection, the chain segments first diffuse towards another reactive site and then connect *via* BER. The reaction rate k_1 (mol/s) for the chain connection (k_1) can be written as:

$$k_1^{-1} = N_A t_1 + N_A t_{BER}, \text{with } t_{BER} = t_{0\_BER}\exp\left[\frac{E_{ab}}{R(T+273)}\right] \tag{7a}$$

where t_1 is the traveling time of a segment with i monomers to meet another reactive site at segment tails. Following our previous work [48], $t_1 = \tau_i (C_r N_A b^3)^{-4/3}$, with τ_i being the Rouse time of the segment i monomers, C_r being the concentration of segments at a continuum point, and b being the monomer length. t_{BER} is the average time spent on a BER, with E_{ab} being the BER energy barrier, and t_{0_BER} being a time constant.

For the chain cleavage reaction, the solvent molecules first diffuse towards an ester bond on the chain backbone and then break the chain *via* BER. The reaction rate k_2 (mol/s) for the chain can be written as:

$$k_2^{-1} = N_A t_2 + N_A t_{BER} \tag{7b}$$

where t_2 is the traveling time of the solvent molecule. $t_2 = \langle r_2 \rangle^2 / D_s$, with $\langle r_2 \rangle$ being the average distance between an ester and solvent molecule. According to the theory of mean inter-particle distance, $\langle r_2 \rangle = \sqrt[3]{4\pi C_s N_A / 3}$.

On the other hand, Eq. (7a) implies that the repolymerization rate is only dependent on the local concentration of monomers, without considering their long-range diffusion within the system. In this model, we assume that the diffusion of monomers is very slow, and therefore, we do not take into account the potential impact of their diffusivity. However, when extending the modeling approach to different systems involving small molecule reactants, considering the long-range diffusion of monomers may be necessary. Additionally, it will be important to identify the gelation point of the matrix resin. Beyond the gelation point, the motion of larger molecular oligomers becomes coordinated within the system, which is fundamentally different from the diffusion of smaller monomers and may have a significant influence on the overall network repolymerization kinetics.

The rate constants are then employed in first-order reaction equations to model the content and length distribution of chain segments during the repolymerization process. As illustrated in the Supplementary Materials (Section S3), four types of BERs influence the content of segments with i monomers: (a) a segment with i monomers reacts with an EG molecule, breaking into two shorter segments; (b) a segment with i monomers reacts with another chain segment, resulting in the formation of a longer chain segment and generating a new EG molecule; (c) two shorter chain segments react, forming a segment with i monomers and generating a new EG molecule; (d) a long chain segment reacts with an EG molecule, forming a segment with i monomers and another chain segment. At time t during the repolymerization process, the content of chain segments with i monomers, C_i, is determined as the summation of the reaction rates from these four reactions:

$$\dot{C}_i = \underbrace{-k_2 C_i}_{r_i^a} \underbrace{-k_1 C_i}_{r_i^b} + \underbrace{k_1 \sum_{j=1}^{i-1} C_j \left(C_{i-j} \Big/ \sum\nolimits_m C_m \right)}_{r_i^c} + \underbrace{k_2 \sum_{j=i+1}^{N_\infty} C_j (2/(j-1))}_{r_i^d} \tag{8}$$

Solving the above differential equations will determine the content and length distribution of chain segments, as well as the content of solvent molecules. The average chain segment length can be formulated as:

$$N_{ave}(t) = \frac{\sum_{i=1}^{N_\infty} i C_i}{\sum_{i=1}^{N_\infty} C_i} \tag{9}$$

The degree of curing, P, which serves as the bridge between the microscale network structure and macroscopic material properties, is defined based on the amount of ester groups on the segment backbone, $\sum_{i=2}(i-1)C_i(t)$, normalized by its final value in the fully polymerized network:

$$P = \frac{\sum_{i=2}^{N_\infty} (i-1) C_i}{(N_\infty - 1) C_{N_\infty}} \tag{10}$$

In the initial state, the system contains only the fully depolymerized segments ($i = 1$) without ester bonds, so the network repolymerization degree is zero. When the network is full cured, we assume that all chain segments are linked to form long chains with a uniform maximum length denoted as N_∞, and their volume fraction is C_{N_∞}. In this scenario, the network repolymerization degree is one.

The reaction rates of four possible reactions in Fig. S3 also determine the changing rate of solvent content (C_s) at a material point mentioned in Eq. (4) as:

$$k_s(\boldsymbol{x}, t) = \sum\nolimits_{i=1} \left(r_i^a - r_i^b + r_i^c - r_i^d \right) \tag{11}$$

3.4. Finite element modeling approach

In the realm of FEA computational studies, there exists a wealth of research to address the coupled diffusion reaction problems [56–61]. While these investigations have greatly advanced our understanding of multifaceted phenomena, our approach in this study takes a simplified path for analytical convenience. We assume that the processes of solvent transport and the development of the mechanical stress field are uncoupled in each numerical step. This choice is underpinned by two key considerations: first, the solvent transportation within the system is extremely slow compared to the pace of chemical reactions. Within each numerical step, the local solvent content within the finite elements can be safely considered as a constant. Secondly, the magnitude of the stress field generated during the repolymerization process is relatively small, which is unlikely to exert a significant influence on the ongoing chemical reactions.

The diffusion partial differential equations (Eqs. (1) and (2)) are solved using a customized finite element code in MATLAB with 2D triangular elements. The solvent content at the finite element nodes at $\boldsymbol{x}$ (x_1, x_2, x_3) is represented by the vector $\boldsymbol{c} = [C_{s1}, \ldots C_{sn}]$, with n being the number of nodes in each element. The element governing equation is written as:in the above equations, $\boldsymbol{N} = [N_1(x_1, x_2, x_3), \ldots N_n(x_1, x_2, x_3)]$ is the shape function of the adopted finite elements. $\boldsymbol{B}$ is the element shape matrix with $B_{ij} = \partial N_i / \partial x_j$. $\boldsymbol{D}$ is the diffusivity matrix. With the assumption of isotropic materials, we have $D_{ij} = D_s \delta_{ij}$.

On the surface of the model, the solvent evaporation imposes a natural boundary condition, which can be formulated as:

$$D_s \frac{dC_s}{d\boldsymbol{n}} = -J_e = -K_s C_s \tag{13}$$

The development of stress field modeled as a static problem within each numerical step. The displacement vector at the nodes at $\boldsymbol{x}$(x_1, x_2, x_3) is $\boldsymbol{d} = [u_{11}, u_{12} \ldots u_{n1}, u_{n2}]$. Without considering surface pressure or body force, the element governing equation is written

$$\boldsymbol{k}_C \boldsymbol{d} = 0 \tag{14a}$$

$$with\ \boldsymbol{k}_C = \iiint_V \boldsymbol{B}\boldsymbol{C}\boldsymbol{B}^T dV \tag{14b}$$

$\boldsymbol{C}$ is the elasticity matrix for 2D plane strain problem.

During the numerical analysis, the solvent content of each element is initially calculated based on Eq. (4), incorporating the solvent evaporation boundary condition described in Eq. (13). Subsequently, the content and average length of chain segments are updated by the microscale reaction kinetics equations (Eqs. (7), (9) and (10)), which serve as internal state variables. These state variables are then utilized to compute the network modulus, volume shrinkage strain, and stress relaxation time using Eqs. (1)–(3). The development of the stress field within the FEA model is determined using Eq. (14). To ensure the calculations on Cauchy stress in the current configuration, node displacement and current positions are updated in each numerical step, which is used to create the reference configuration and calculations on the new stress values.

4. Results and discussions

4.1. Repolymerization kinetics and properties of epoxy matrix

The repolymerization kinetics and property evolutions of epoxy matrix were first investigated with several key experiments to determine model parameters. First, a fully cured epoxy sample was subjected to swelling tests in EG solvent. Fig. 3a presents the normalized mass increment and diffusivity as functions of temperature. This dataset enabled the determination of the reference solvent diffusivity D_{s0} =

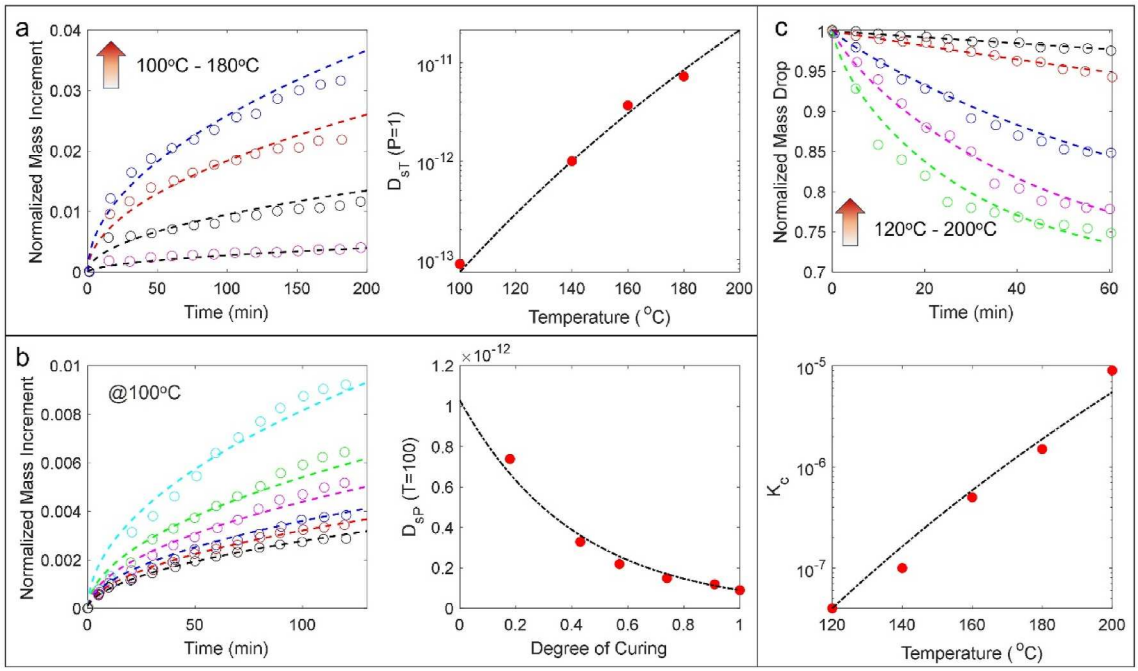

Fig. 3. Epoxy characterization at varied temperatures and degrees of curing. (a) Mass increment and diffusivity of fully cured epoxy at different temperatures. (b) Mass increment and diffusivity of epoxy with varying degrees of curing, conducted at a testing temperature of 100 °C. (c) Mass dropping rate of depolymerized epoxy solution during the solvent evaporation process, alongside the corresponding measured mass transfer coefficients at different temperatures.

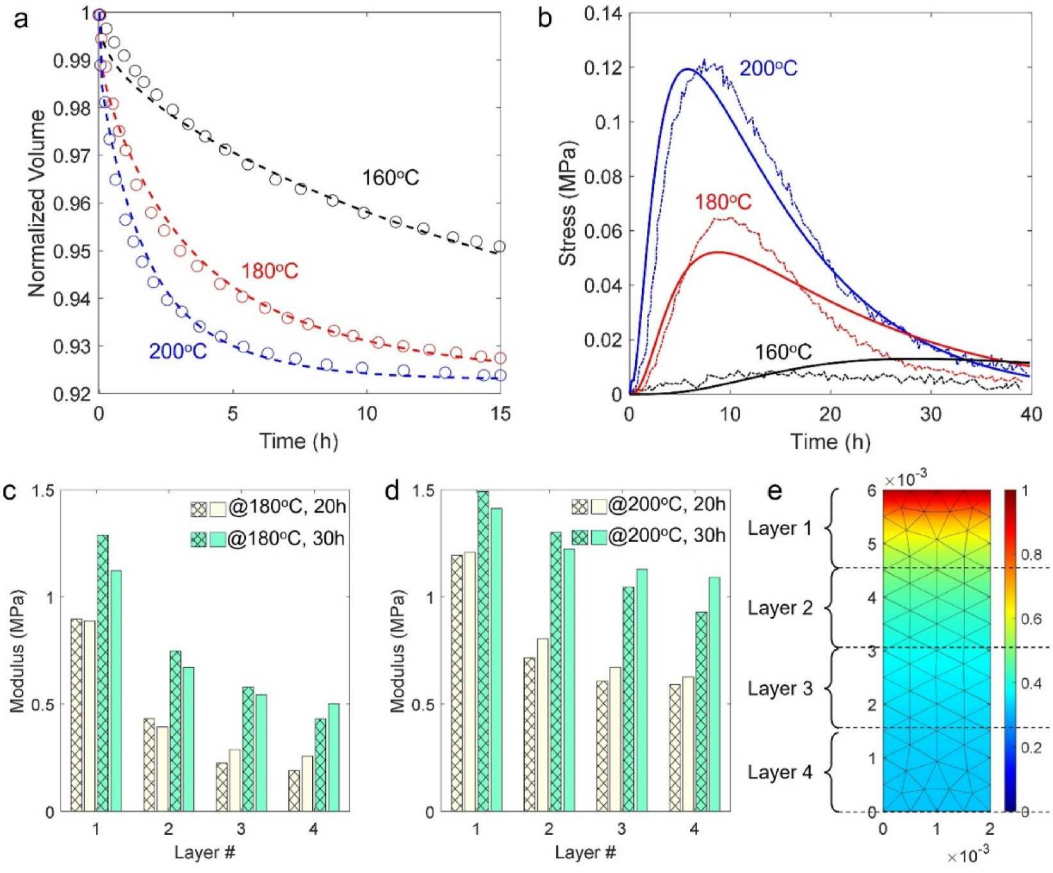

Fig. 4. Predictions and experimental data for re-polymerization and stress evolution in epoxy. (a) Predictions of network volume change during re-polymerization. Dashed lines represent model predictions, while dots represent experimental data. (b) Evolution of residual stress during the re-polymerization of epoxy samples. Solid lines denote model predictions, and dashed lines represent experimental data. Network modulus evolution in the first four curing layers during bulk epoxy re-polymerization at (c) 180 °C and (d) 200 °C. (e) Simulated network degree of curing after heating at 180 °C for 30 h.

10^{-12} m^2/s at 140 °C and the energy barrier $E_s = 83.2$ kJ/mol in Eq. (4b).

Second, elastic moduli of epoxy samples after being heated for different times were tested, which determined the network degree of curing using Eq. (2b) with $\alpha = 0.16$. Subsequently, these samples were subjected to swelling tests at 100 °C. The normalized mass increment and the diffusivity are presented in Fig. 3b as a function of temperatures. This dataset determined the scaling factor for solvent diffusivity in Eq. (4b) as $\beta = 0.437$.

Third, the depolymerized polymer solution was heated at a specific temperature, and the mass loss due to EG solvent evaporation was recorded over time. As shown in Fig. 3c, each curve at a distinct temperature is used to determine the mass transfer coefficient, K_c (m/s), for solvent evaporation, which subsequently determined the reference mass transfer coefficient $K_{s0} = 4 \times 10^{-8}$ m/s at 140 °C and the energy barrier $E_k = 95$ kJ/mol in Eq. (5b).

The evolution of the volume shrinkage strain of the epoxy network during the repolymerization process was characterized. Initially, the depolymerized polymer solution was heated to 200 °C. After the samples reached a state of gelation, they were subsequently transferred to the DMA tester. Measurements of volume shrinkage were taken at temperatures of 160 °C, 180 °C, and 200 °C, respectively. The experimental data is plotted in Fig. 4a as dots.

The experimental results show that the rate of volume shrinkage increases with the repolymerization temperature. Specifically, at 200 °C, the sample's volume reduces by approximately 8% after being heated for 6 h. The degree of the subsequent volume shrinkage does not change notably, which suggests near-complete repolymerization of the epoxy network. The observed volume shrinkage is attributed to two mechanisms, namely (i) the solvent evaporation and (ii) the transition of weak Van-der-Waals interactions among chain segments into covalent bonding. These two mechanisms are mathematically formulated in Eq. (6b), incorporating weight factors denoted as w_1 and w_2, respectively. Upon setting $w_1 = 0.2$ and $w_2 = 0.8$, it is observed that the model predictions (represented by solid lines in the figure) closely align with the experimental results across different temperatures.

When the repolymerization process takes place within a confined environment, the tendency of network volume shrinkage results in the development of residual stress within the epoxy matrix, which is a notable concern in the manufacturing of thermoset composites. The experimentally measured residual stress is plotted as a function of heating time in Fig. 4b. It is seen that during the early stages of repolymerization, the residual stress increases almost linearly due to solvent evaporation and network shrinkage. However, since the TBD catalyst does not evaporate, the network can undergo transesterification BERs, which effectively releases the internal stress. Consequently, the internal stress starts to decrease after reaching its peak value. This phenomenon suggests that the connections of chain segments and the network repolymerization are faster mechanisms compared to the bond exchanges among macromolecular polymer chains.

While the internal stress in the epoxy networks can eventually be released, the peak stress varies at different repolymerization temperatures. For instance, at 200 °C, the peak stress can reach 0.12 MPa due to the faster volume shrinkage of the network, which will likely result in sample failure with restrained boundary conditions, especially when the temperature significantly exceeds the network's transition temperature, and the material is brittle. On the other hand, lower temperatures result in the gradual development of residual stress that can be readily released by BERs, but the overall repolymerization process is slow. The solid lines in Fig. 4b represent the predictions of the modeling framework. By adjusting the scaling factor ξ of Eq. (3) to be 4.62×10^5, the developed model can precisely capture evolution of residual stress and peak stress during the repolymerization at different temperatures.

All the material parameters involved in the modeling framework are listed in Table 1. With the determined parameters, the thermomechanical properties of the bulk repolymerizing samples with nonuniform curing degrees along the thickness direction were studied. The evolutions of the elastic moduli of the first four curing layers close to the top surface are plotted in Fig. 4c and d, wherein the repolymerization temperature is 180 °C and 200 °C, respectively. The close comparison suggests that the developed constitutive modeling framework is efficient to capture the nonuniform distribution of material properties during the repolymerization of bulk epoxy samples.

Table 1
All the material parameters in the modeling framework.

Parameters	Values	Description
Continuum-level modeling		
•*Stress-strain relationships*		
E_∞	1.5 MPa	Equilibrium modulus of a fully cured network
α	0.16	Scaling factor betwee network modulus and curing dergee
ξ	4.62×10^5	Scaling factor of network stress relaxation time
•*Solvent transportation*		
D_{s0}	1×10^{-12} m^2/s	Reference solvent diffusivity
β	0.437	Scaling factor for solvent diffusivity
E_s	83.2 kJ/mol	Activation energy for solvent diffusion
R	8.31 $Jmol^{-1}K^{-1}$	Gas constant
•*Solvent evaporation*		
K_{s0}	4×10^{-8} m/s	Reference value of mass transfer coefficient K_c
E_k	95 kJ/mol	Activation energy of K_c
•*Network volume shrinkage*		
w_1	0.2	Weight coefficient for the contronution of solvent content
w_2	0.8	Weight coefficient for the contronution of network polymerization
M_s	116.88 g/mol	Solvent molecular weight
ρ_s	1.11×10^6 g/m^3	Solvent density
Microscale chain cleavage and reconnections		
b	1 nm	Average length of monomers
t_{0_BER}	3.23×10^{-2} s	Time constant for BERs
E_{ab}	8.15 kJ/mol	Energy barrier for BERs
τ_{0s}	60 s	Rouse time of the shortest chain segment
N_∞	10	Number of monomers between two crosslinkers

From the figure, it is observed that the first curing layer on the top surface of the epoxy sample polymerizes first. With sufficient heating time (e.g., ~30 h at 200 °C), the modulus of the first curing layer reaches the same level as the unprocessed sample (~1.5 MPa). Increasing temperature from 180 °C to 200 °C increases the curing speed of each layer, but the delay in the repolymerization between the first and the rest curing layers tends to be the same. In other words, a higher temperature did not lead to more uniform material properties during the process. This is because after a stiff curing layer quickly formed on the surface (Fig. 4e), which blocks the transportation of the solvent molecules due to the lower solvent diffusivity and thus suppresses the curing of the bottom materials.

4.2. Repolymerization kinetics of composite lamina: a reduced-order computational model

Applying the effective parameters, the developed FEA computational model is utilized to study the repolymerization process of fabricated composites containing 37% carbon fiber. A significant challenge arises when attempting to accurately model the arrangement of fibers within the composite and establish the model itself. For instance, in the case of the 37% composites with a thickness of 3 mm, each carbon fiber has a diameter of 7 μm. Within a 3 mm-by-3mm cross-sectional area, there exist over thirty thousand fibers. A comparable mesh size as the fiber diameter would yield millions of elements, which poses challenges for both meshing the model and conducting FEA simulations.

To tackle this challenge, we examined the effectiveness of several reduced-size FEA models. In our recent computational study [62], it was

revealed that the randomness of fiber positioning over the composite cross-section has a negligible influence on solvent diffusion and the composite recycling kinetics. As a result, in this study, we assume that the fibers are neatly arranged with even spacing. Consequently, the reduced-size FEA model considers only a half strip along the composite thickness direction, with symmetric boundary conditions applied. The model height (1.5 mm) is half of the sample thickness, and solvent evaporation boundary conditions are applied to the top surface.

With a fixed height of the FEA model, the diameter of the embedded fibers is varied, while their total volume fraction is kept at 37%. When using a larger diameter for the equivalent fiber, the required amount of fiber decreases, and the FEA model is simplified. In the **Supplemental Material** (Section S4), we present a comparison of the simulated repolymerization processes using these reduced-size FEA models. Specifically, we tracked the evolution of the matrix curing degree and the changes in peak stress around the carbon fiber. The results reveal that as the amount of fiber increases from one, the repolymerization process slows down. However, when the fiber count is more than seven, the evolutions of curing degree and peak stress are close to each other, which suggests a convergence of the sizing effect for the FEA model. This also suggests that the blocking effect of fiber on composite recycling might be independent of fiber diameter, depending only on the fiber volume fraction.

Based on this comparative analysis, the FEA model with seven carbon fibers is utilized for subsequent computational studies, as shown in Fig. 5a. For composites featuring 37% carbon fiber, the diameter of the equivalent fiber is set at 71 μm. In addition to the model and boundary conditions, the figure also marks several tracking nodes that are of particular interest for studying the repolymerization process. Tracking nodes A1 through A8 are on the left side of the model and are employed to investigate the progress of the matrix curing degree. Meanwhile, tracking nodes B1 through B7 are positioned along the top of the fiber, and nodes C1 through C7 are located on the side of the fiber. These sets of nodes are placed at locations with intense stress concentration.

Fig. 5b shows the evolution of the material curing degree at Tracking nodes A1 through A8. It is observed that the initial curing speed at each of these nodes remains constant. Later the increments slow down due to the reduced solvent diffusivity and a slower chain connection rate within the curing network. Tracking node A1 on the top surface exhibits the highest curing degree over time. The remaining tracking nodes experience delayed curing processes, but their differences in the evolution of curing degree are getting smaller. This phenomenon is attributed to the blocking effect of top curing layers on the diffusion-reaction process.

Fig. 5c shows the evolution of Mises stress at Tracking nodes B1 through B7 and C1 through C7. Several interesting observations can be made. First, stress values at these nodes initially increase due to solvent evaporation-induced volume shrinkage, followed by a subsequent decrease because of BER-induced stress relaxation. For carbon fibers located near the evaporation surface, there is a higher stress concentration on the top side compared to the left side (B_i v.s. C_i). In contrast, a carbon fiber located deeper within the composite material exhibits similar stress values on both the top and left sides. Second, as moving deeper into the composite material, the magnitude of the peak stress around the fiber is getting smaller. This happens primarily because BERs release significant stress before the curing front reaches the specific location and introduces substantial volume shrinkage. Third, it is important to note that a curing degree close to one does not necessarily mean that the composites are ready for use. There is still significant stress concentration around the fiber. The distributions of Mises stress and curing degree for the top unit cell are shown in Fig. 5d and e, respectively. After being heated at 180 °C for 12 h, it is evident that most of the resin is fully cured, namely the chain lengths have reached their maximum level. However, stress levels around the fiber remain significant. Considering the modulus of fully cured epoxy is around 1.5 MPa, the stress concentration of 0.14 MPa corresponds to roughly a 10% strain. Unloading at this stage would likely lead to crack propagation and fiber debonding from the matrix material. These simulation results suggest that, in addition to the matrix curing degree, it is also essential to consider the residual stress within the composite when determining the required heating time.

After heating the samples at a specific temperature for a given time, the composite lamina is stretched in the transverse direction to assess its modulus. Fig. 5f shows the transverse modulus of the composite lamina, normalized by the value of an as-fabricated sample (2.1 MPa), in both experiments and simulations. In the simulations, the FEA model is

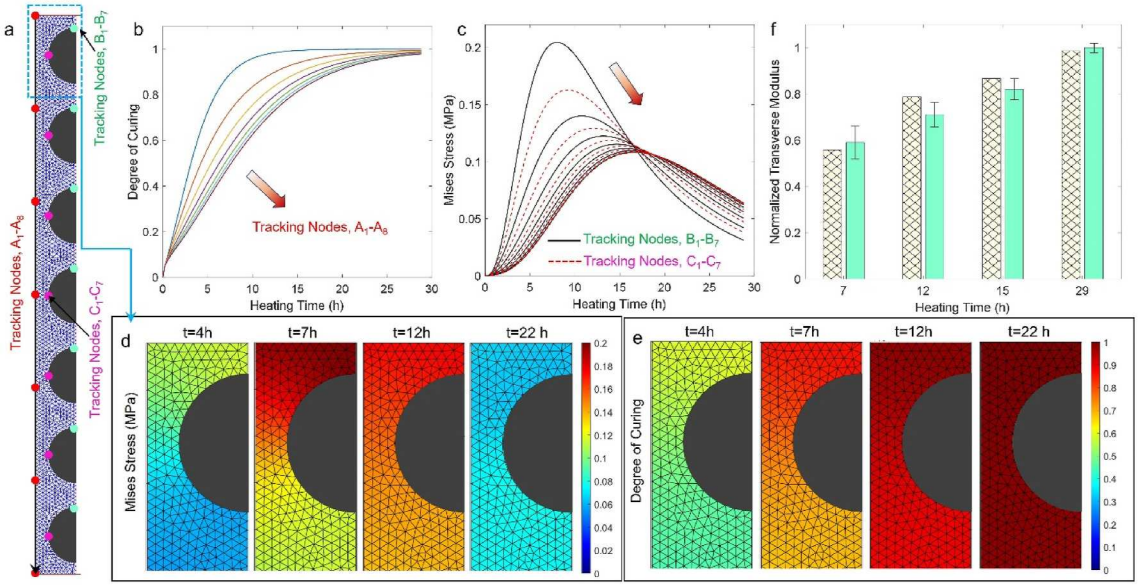

Fig. 5. Computational model details and simulation results. (a) The reduced-size FEA computational model with seven equivalent fibers aligned in the thickness direction. The fiber volume fraction is 37%, and the model height is 1.5 mm, with an equivalent fiber diameter of 71 μm. (b) Evolution of degrees of curing at 180 °C at eight Tracking nodes (A1-A8) marked in Figure a. (c) Evolution of local Mises stress at 180 °C at Tracking nodes (B1–B7 and C1–C7). (d) Simulated distributions of Mises stress around the first carbon fiber within the FEA model. (e) Simulated distributions of matrix degree of curing around the first carbon fiber within the FEA model. (f) Predicted normalized transverse modulus at various heating times at 180 °C.

subjected to a displacement boundary condition in the horizontal directions. Stress responses are calculated, and the modulus is determined within the initial 1% strain. It is seen that the model closely captures the experimental results without any parameter adjustments involved, which proves the effectiveness of the developed computational model and associated parameter in studying the repolymerization process of composite materials.

4.3. Parametric study to reveal the repolymerization mechanisms

4.3.1. Influence of fiber volume fraction and heating temperature

The reduced-size FEA model with seven equivalent carbon fiber is employed to conduct parametric computational studies to examine the influences of fiber volume fraction and temperature on the repolymerization process. Fig. 6a shows the required heating time, defined as the point at which the degree of curing for all elements exceeds 0.9 and the Mises stress for all elements falls below 0.05 MPa. The figure also presents the energy consumption associated with the repolymerization process. In this study, heating of the composite samples was carried out using a 1.9 cu. ft. oven (Across International, NJ, USA) with an approximate surface area of 0.14 m^2. The energy consumption was estimated by calculating the heat loss during free natural convection of the oven at a constant temperature. The heat transfer coefficient for the metal is assumed to be 20 W/(m^2K). Based on the Newton's Law of Cooling, the required energy input is calculated as the heating time multiplied by the surface area and the temperature difference between the oven and room temperature.

The results indicate that with a constant fiber volume fraction, the required heating time for the composite repolymerization initially decreases as the heating temperature rises and then undergoes a slight increase. For instance, at a fiber content of 60%, the shortest heating time is approximately 25 h at 230 °C, whereas at 260 °C, the required heating time for complete repolymerization extends to 33 h. The initial reduction in heating time can be attributed to the accelerated solvent diffusion and chain connection reactions at higher temperatures, resulting in a faster curing process. However, when the temperature is significantly increased to 260 °C, the uppermost layers cure first, forming a rigid material that blocks solvent evaporation and hinders the curing of the epoxy layers beneath them.

Another important factor contributing to this trend is the high stress concentration developed around the carbon fiber. Fig. 6b plots the matrix curing degree at Tracking node A8 and the evolution of the Mises stress at Tracking node B1. At 260 °C, although the matrix material can be fully cured relatively quickly within 7 h, the peak stress around the carbon fiber remains notably high at approximately 0.35 MPa. As a result, additional heating time is needed for the BERs to release the internal stress and meet the criteria for minimal residual stress after repolymerization. The extended heating time results in a significant increase in energy consumption. As shown in Fig. 6a, the lowest energy consumption at 190 °C is around 12 kJ, while it nearly doubles to 23 kJ at 260 °C. Conversely, at lower temperatures, where the peak stress during repolymerization remains relatively low at around 0.05 MPa, the overall network curing process is slow, which leads to an extended heating time and higher energy consumption.

Additionally, Fig. 6a highlights that the fiber content influences the repolymerization speed at lower temperatures, particularly below 190 °C. At these lower temperatures, the presence of fiber significantly blocks the diffusion of solvent and thus reduces the rate of chain connections. Fig. 6c plots the evolutions of the matrix curing degree at Tracking node A8 and the evolutions of the Mises stress at Tracking node B1. It is shown that a higher fiber volume fraction delays the curing process of the matrix material, but the overall peak stress remains relatively consistent across different cases. Above 190 °C, solvent diffusivity is no longer the limiting factor. The overall repolymerization process becomes predominantly governed by temperature. As a result, all cases exhibit nearly identical required heating times.

4.3.2. Influence of solvent diffusivity and heating temperature

Parametric computational studies were conducted to investigate the effects of solvent diffusivity and heating temperatures on the

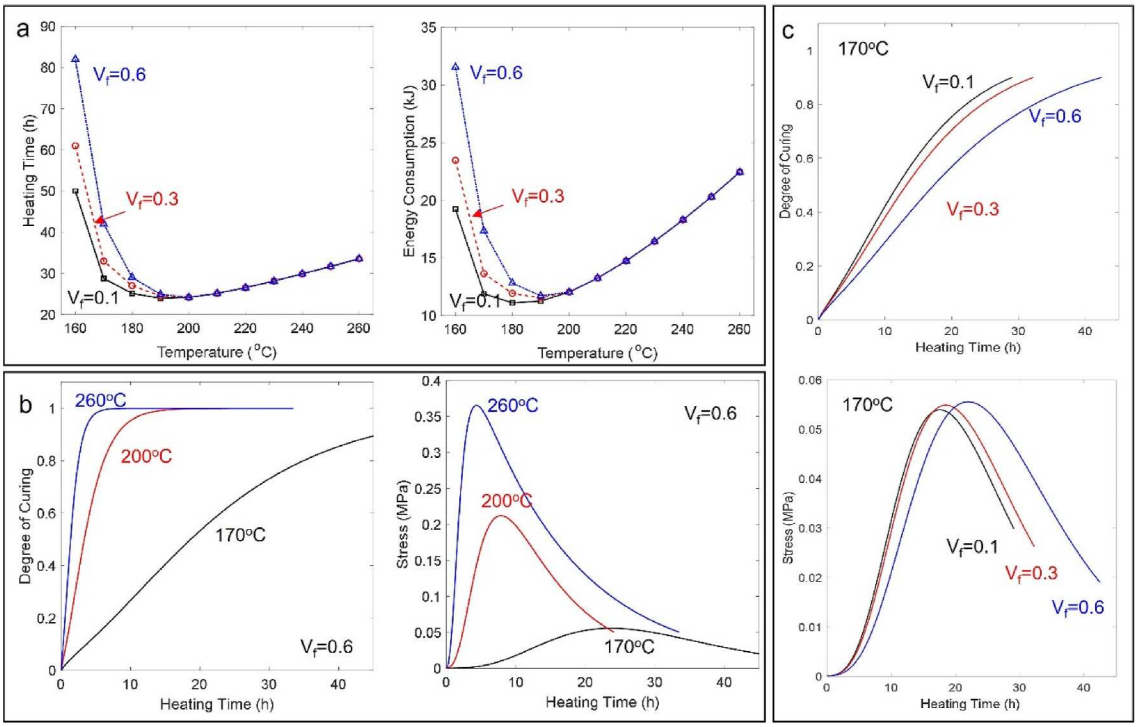

Fig. 6. Parametric study results. (a) The required heating time and energy consumption as functions of heating temperature and fiber volume fractions. (b) Evolutions of the degree of curing at tracking node A8 and (c) evolutions of local stress concentration at tracking node B1. In Figure a, the fiber volume fraction is held constant while varying the heating temperature. In Figure b, the heating temperature is kept constant while varying the fiber volume fraction.

repolymerization of composites with a 37% carbon fiber content. In the experimental case, the reference diffusivity at 140 °C was determined to be $D_{s0} = 10^{-12}$ m^2/s. Throughout the parametric studies, this reference diffusivity varied within the range of $0.01D_{s0}$ to D_{s0}. Their temperature dependency still follows the same Arrhenius-type superposition rule. The corresponding reference mass transfer coefficient is changed by the same magnitude compared to the experimental case. Lower diffusivity corresponds to the use of solvents with a higher molecular weight or a lower solubility in the epoxy matrix, as indicated in our previous research [50]. The temperature range for these parametric studies is extended from 170 °C to 210 °C. Fig. 7a shows a contour plot of the required heating time for complete repolymerization with >0.9 matrix curing degree and <0.05 MPa residual stress, while Fig. 7b displays the peak stress during the repolymerization process on the top side of the first carbon fiber (at Tracking node B1), near the evaporation surface.

The simulation results reveal that the repolymerization rate increases with higher solvent diffusivity and temperature. A higher solvent diffusivity allows the EG molecules generated after chain connection reactions to rapidly diffuse out of the system, thereby shifting the system equilibrium toward repolymerization. An elevated temperature not only enhances the solvent diffusion and evaporation but also accelerates the BERs for chain connection reactions. The parametric studies also reveal the distinct zones for the influences of solvent diffusivity and temperature. The boundary between these zones is highlighted with white dashed lines in Fig. 7a. Within Domain I, lower solvent diffusivity results in significantly longer heating times required to completely repolymerize the epoxy matrix. This occurs because a substantial quantity of EG molecules is generated and accumulates within the system, inhibiting chain connection reactions and promoting chain cleavage. Increasing the temperature in these cases does not significantly promote the repolymerization speed. Therefore, within Domain I, the limiting factor for the repolymerization process is solvent diffusivity.

The overall repolymerization speed within Domain II increases with temperature, indicating that temperature becomes the limiting factor. However, when it comes to Domain III, the decreases in the required heating time are less pronounced. This is primarily due to the high peaks stress levels developed within the model, as shown in Fig. 7b. In comparison to the cases in Domain I, the peak stress within Domain III increases to approximately 0.22 MPa, representing a fivefold increment. This requires additional heating time to fully release the internal residual stress. Consequently, the limiting factor for the overall recycling speed in Domain III shifts from insufficient temperature to excessive stress concentration developed around the fiber.

To further clarify the underlying mechanisms, four representative cases have been selected from the parametric studies, which are marked in Fig. 7a. Their evolutions of network curing degrees on Node A8 and the evolutions of Mises stress on Node B1 are respectively plotted in Fig. 7c and d. For Case ① that is located near the boundary of Domain I, the processing conditions involve a lower temperature (180 °C) and a low diffusivity ($0.03D_{s0}$). The curing process notably extends to approximately 150 h. Given the low peak stress of 0.75 MPa within the composites, the slow repolymerization process is primarily attributed to slow solvent transportation, evaporation, and chain connection reactions. In case ②, the temperature is increased to 210 °C, and the solvent diffusivity reaches D_{s0}. While most of the matrix materials achieve a curing degree above 90% within 5 h of heating, the peak stress

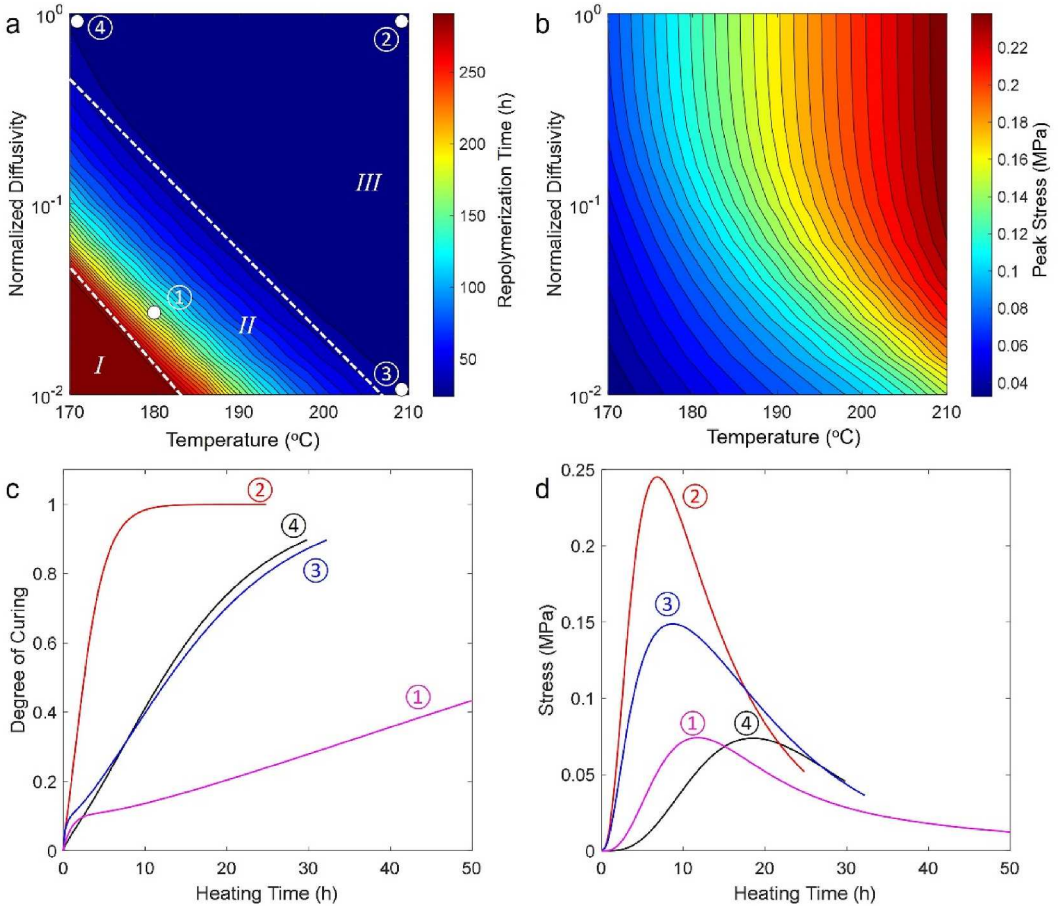

Fig. 7. Parametric study results at 200 °C with different heating times and solvent diffusivities. (a) Contour plot illustrating the required heating time for complete curing of the composite lamina. (b) Contour plot depicting the peak stress within the FEA model. (c) Evolution of the degree of curing at tracking node A8. (d) Evolution of local stress concentration at tracking node B1. Repolymerization conditions for the four cases are indicated in Figure (a).

around the fiber is up to 0.25 MPa. This elevated stress increases the risk of matrix fracture and fiber/matrix debonding. An additional 20 h of heating is required to fully release the accumulated stresses, extending the overall heating time significantly.

In comparison, Case ③ uses the same temperature of 210 °C, but with a much lower solvent diffusivity of 0.01 D_{s0}. In this case, the peak stress is reduced to 0.15 MPa, with the overall heating time maintained around 30 h. The optimal processing condition revealed in the figure is for Case ④, where the temperature is 170 °C, and the solvent diffusivity is D_{s0}. Despite the lower processing temperature compared to Case ③, the sample is still able to be fully cured within 30 h, and the highest peak stress is significantly lower at 0.07 MPa. Furthermore, the curing speed of the top surface at the moderate temperature is slower, which encourages solvent transportation and evaporation, and promotes the overall sample repolymerization speed. These conditions are considered both safe and energy-efficient for composite manufacturing. The comparison between Case ④ and Case ③ also suggests that, when it comes to reducing the residual stress within composites while maintaining overall repolymerization efficiency, lowering the temperature is a more effective approach than reducing solvent diffusivity.

4.3.3. *Influence of reaction rate and heating temperature*

The effects of BER rate and heating temperatures on the repolymerization of composites with 37% carbon fiber have also been studied. Within the developed computational model, the rates of BER-induced chain connection and cleavage are formulated in Eq. (7a) and Eq. (7b), respectively. During the parametric studies, these reaction rates are both multiplied by a dimensionless factor, the normalized reaction rate (f_k), which varies from 0.1 to 3.1. A higher factor indicates a higher BER reactivity at equivalent temperatures. This can be achieved by increasing the catalyst content in the fabricated epoxy network or by using other dynamic covalent bonds with lower activation barriers. The temperature range for these parametric studies extends from 170 °C to 260 °C. Fig. 8a presents a contour plot of the required heating time for full repolymerization, while Fig. 8b displays the peak stress during the repolymerization process on the top side of the first carbon fiber at Tracking node B1.

The results indicate that increasing the reactivity of the BER and temperature both have equivalent effects in promoting the repolymerization speed. Similar to the previous section, the contour plot in Fig. 8a also reveals three distinct domains of influence: one dominated by reactivity, one by temperature, and one by the high residual stress around the carbon fiber. Four representative cases have been selected from the parametric studies and are marked in Fig. 8a. The evolutions of network curing degrees on Node A8 and the evolutions of Mises stress on Node B1 are respectively plotted in Fig. 8c and d. It also reveals that the optimal material and processing conditions are located on the top-left corner of the contour plot, as indicated by Case ④. The high reactivity enhances chain connection reactions and overall repolymerization kinetics. The relatively low processing temperatures help prevent the development of intense stress concentration around the fiber and reduce the additional heating time required for stress relaxation. It also mitigates the formation of a top surface film, thereby promoting solvent evaporation from the composite surface.

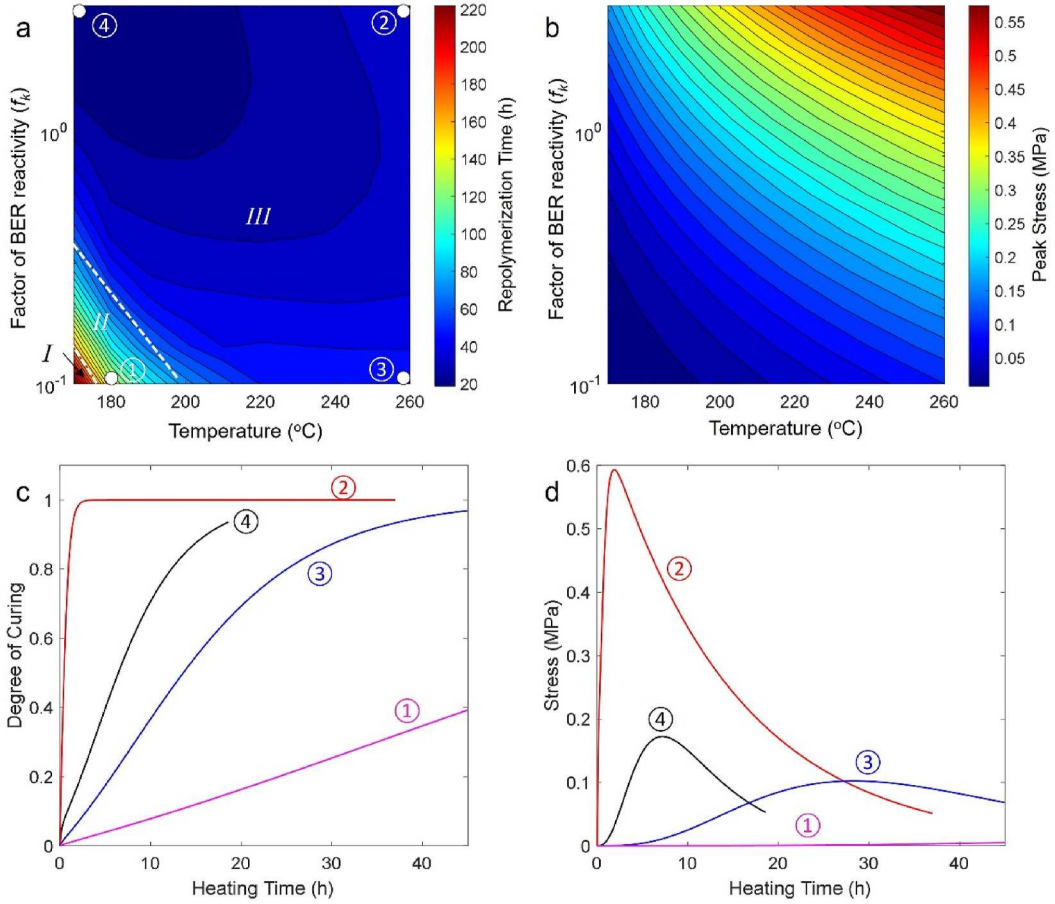

Fig. 8. Parametric study results at 200 °C with different heating times and reactivity. (a) Contour plot of the required heating time for complete curing of the composite lamina. (b) Contour plot of the peak stress within the FEA model. (c) Evolution of the degree of curing at tracking node A8. (d) Evolution of local stress concentration at tracking node B1. Repolymerization conditions for the four cases are indicated in Figure (a).

5. Conclusion

In this study, a physics-based computational model that integrates diffusion-reaction-mechanics principles is developed to study the solvent evaporation-induced repolymerization mechanisms of epoxy composites embedded with carbon fiber. The finite-element modeling framework establishes connections between microscale bond-exchange kinetics, solvent diffusion and evaporation, and continuum-level composite properties, including the degree of curing in the matrix and stress concentrations around the carbon fiber. The model shows close predictions on the experimental data of the network volume shrinkage, residual stress development, and transverse modulus of repolymerized composite lamina. It is then applied to performance computational parametric studies to reveal the influences of different material and processing conditions on the composite repolymerization behaviors.

A notable finding in this study is the intricate relationship between temperature and the time required for complete repolymerization. Initially, as temperature increases, the time needed for repolymerization decreases, but beyond a certain point, it starts to increase again. This phenomenon can be attributed to two key factors. First, at higher temperatures, a rigid surface film forms quickly, impeding the curing of the resin beneath it. Second, increased temperatures lead to the development of intense stress concentrations around the carbon fiber, requiring additional heating time for stress release. The presence of carbon fiber can also significantly block solvent transportation, reducing the overall repolymerization speed. However, this effect is most pronounced at relatively low processing temperatures, where solvent diffusion dominates the process. Solvent diffusivity and BER reactivity exhibit similar influences on the required heating time. The contour plots illustrate three distinct domains of influence, each primarily dominated by either reactivity, temperature, or the high residual stress around the carbon fiber. The optimal processing conditions are characterized by relatively lower temperatures and higher solvent diffusivity or BER reactivity. These conditions not only facilitate rapid resin curing but also mitigate the development of intense stress concentrations around the fiber.

Overall, this computational study substantially advances our understanding of the intricate mechanisms involved in recycling composites using organic solvents. It provides valuable theoretical insights and practical guidance for industrial stakeholders aiming to optimize processing conditions and promote the commercialization and widespread adoption of this innovative recycling technique, thereby contributing to the sustainable development of society.

CRediT authorship contribution statement

Christopher Chung: Writing – original draft, Visualization, Methodology, Conceptualization. **Huan Jiang:** Writing – original draft, Visualization, Investigation. **Chaoqian Luo:** Visualization, Investigation. **Kai Yu:** Writing – review & editing, Supervision, Project administration, Funding acquisition, Conceptualization.

Declaration of competing interest

The authors declare the following financial interests/personal relationships which may be considered as potential competing interests: Kai Yu reports financial support was provided by National Science Foundation. If there are other authors, they declare that they have no known competing financial interests or personal relationships that could have appeared to influence the work reported in this paper.

Data availability

Data will be made available on request.

Acknowledgments

K.Y. acknowledges the support from the National Science Foundation (grant CMMI-2046611).

Appendix A. Supplementary data

Supplementary data to this article can be found online at https://doi.org/10.1016/j.mtsust.2024.100792.

References

[1] P.K. Mallick, Fiber-Reinforced Composites: Materials, Manufacturing, and Design, third ed., CRC Press, Taylor & Francis Group, Boca Raton, FL, 2007.
[2] D. Chung, Carbon Fiber Composites, Butterworth-Heinemann, Dec 2, 2012.
[3] P. Morgan, Carbon Fibers and Their Composites, CRC Press, May 20, 2005.
[4] V.P. McConnell, Launching the carbon fibre recycling industry, Reinforc Plast 54 (2) (2010) 33–37.
[5] G.N. Hartt, D.P. Carey, Economics of recycling thermosets, SAE Technical Paper 920802, Society of Automobile Engineers (1992). Warrendale, PA.
[6] C.E. Kouparitsas, et al., Recycling of the fibrous fraction of reinforced thermoset composites, Polym. Compos. 23 (4) (2002) 682–689. https://www.sae.org/publications/technical-papers/content/920802/.
[7] K. Ogi, T. Nishikawa, Y. Okano, I. Taketa, Mechanical properties of ABS resin reinforced with recycled CFRP, Adv. Compos. Mater. 16 (2) (2007) 181–194.
[8] S.J. Pickering, Recycling technologies for thermoset composite materials - current status, Compos. Appl. Sci. Manuf. 37 (8) (2006) 1206–1215.
[9] J. Palmer, O.R. Ghita, L. Savage, K.E. Evans, Successful closed-loop recycling of thermoset composites, Compos. Appl. Sci. Manuf. 40 (4) (2009) 490–498.
[10] A. Conroy, S. Halliwell, T. Reynolds, Composite recycling in the construction industry, Compos. Appl. Sci. Manuf. 37 (8) (2006) 1216–1222.
[11] P.T. Williams, A. Cunliffe, N. Jones, Recovery of value-added products from the pyrolytic recycling of glass-fibre-reinforced composite plastic waste, J. Energy Inst. 78 (2) (2005) 51–61.
[12] R.E. Allred, Recycling process for scrap composites and prepregs, SAMPE J. 32 (5) (1996) 46–51.
[13] G. Jiang, et al., Soft ionisation analysis of evolved gas for oxidative decomposition of an epoxy resin/carbon fibre composite, Thermochim. Acta 454 (2) (2007) 109–115.
[14] R.E. Allred, J.M. Gosau, J.M. Shoemaker, Recycling process for carbon/epoxy composites, 2001, A Materials and Processes Odyssey, Books 1 and 2 46 (2001) 179–192.
[15] H.L.H. Yip, S.J. Pickering, C.D. Rudd, Characterisation of carbon fibres recycled from scrap composites using fluidised bed process, Plast., Rubber Compos. 31 (6) (2002) 278–282.
[16] B.J. Jody, et al., A process to recover carbon fibres from polymer matrix composite scrap, Int SAMPE Symp Exhibition 49 (2004) 35–47.
[17] R.E. Allred, A.B. Coons, R.J. Simonson, Properties of carbon fibers reclaimed from composite manufacturing scrap by tertiary recycling, Technology Transfer in a Global Community 28 (1996) 139–150.
[18] M.S. Qureshi, et al., Pyrolysis of plastic waste: opportunities and challenges, J. Anal. Appl. Pyrol. 152 (2020).
[19] I. Vollmer, et al., Beyond mechanical recycling: giving new life to plastic waste, Angew. Chem. Int. Ed. 59 (36) (2020) 15402–15423.
[20] Y.Q. Wang, et al., Chemical recycling of unsaturated polyester resin and its composites via selective cleavage of the ester bond, Green Chem. 17 (9) (2015) 4527–4532.
[21] T. Liu, et al., Mild chemical recycling of aerospace fiber/epoxy composite wastes and utilization of the decomposed resin, Polym. Degrad. Stabil. 139 (2017) 20–27.
[22] A.D. La Rosa, et al., Recycling treatment of carbon fibre/epoxy composites: materials recovery and characterization and environmental impacts through life cycle assessment, Compos. B Eng. 104 (2016) 17–25.
[23] B.J. Adzima, et al., Rheological and chemical analysis of reverse gelation in a covalently cross-linked diels-alder polymer network, Macromolecules 41 (23) (2008) 9112–9117.
[24] M.A. Tasdelen, Diels–Alder "click" reactions: recent applications in polymer and material science, Polym. Chem. 2 (2011) 2133–2145.
[25] K. Yu, et al., Dissolution of covalent adaptable network polymers in organic solvent, J. Mech. Phys. Solid. 109 (2017) 78–94.
[26] C.J. Kloxin, T.F. Scott, B.J. Adzima, C.N. Bowman, Covalent adaptable networks (CANS): a unique paradigm in cross-linked polymers, Macromolecules 43 (6) (2010) 2643–2653.
[27] C.N. Bowman, C.J. Kloxin, Covalent adaptable networks: reversible bond structures incorporated in polymer networks, Angew. Chem. Int. Ed. 51 (18) (2012) 4272–4274.
[28] R.J. Wojtecki, M.A. Meador, S.J. Rowan, Using the dynamic bond to access macroscopically responsive structurally dynamic polymers, Nat. Mater. 10 (1) (2011) 14–27.
[29] Z. Lei, et al., Recyclable and malleable thermosets enabled by activating dormant dynamic linkages, Nat. Chem. 14 (12) (2022) 1399–1404.
[30] C. Luo, et al., Chemomechanics in the moisture-induced malleability of polyimine-based covalent adaptable networks, Macromolecules 51 (23) (2018) 9825–9838.

[31] S. Ma, D.C. Webster, Degradable thermosets based on labile bonds or linkages: a review, Prog. Polym. Sci. 76 (2018) 65–110.
[32] P. Taynton, et al., Heat-or water-driven malleability in a highly recyclable covalent network polymer, Adv. Mater. 26 (23) (2014) 3938–3942.
[33] L. Zhong, et al., Closed-loop recyclable fully bio-based epoxy vitrimers from ferulic acid-derived hyperbranched epoxy resin, Macromolecules 55 (2) (2022) 595–607.
[34] J. Zhang, et al., Itaconic acid-based hyperbranched polymer toughened epoxy resins with rapid stress relaxation, superb solvent resistance and closed-loop recyclability, Green Chem. 24 (18) (2022) 6900–6911.
[35] K. Yu, et al., Carbon fiber reinforced thermoset composite with near 100% recyclability, Adv. Funct. Mater. 26 (33) (2016) 6098–6106.
[36] X. He, et al., Reshapeable, rehealable and recyclable sensor fabricated by direct ink writing of conductive composites based on covalent adaptable network polymers, Int. J. Extrem. Manuf. 4 (1) (2021) 015301.
[37] C. Luo, et al., Chemomechanics of dual-stage reprocessable thermosets, J. Mech. Phys. Solid. 126 (2019) 168–186.
[38] X. He, et al., A sustainable manufacturing method of thermoset composites based on covalent adaptable network polymers, Compos. B Eng. 221 (2021) 109004.
[39] H. Chen, et al., Spiroborate-linked ionic covalent adaptable networks with rapid reprocessability and closed-loop recyclability, J. Am. Chem. Soc. 145 (16) (2023) 9112–9117.
[40] X. He, Z. Lei, W. Zhang, K. Yu, Recyclable 3D printing of polyimine-based covalent adaptable network polymers, 3D Print. Addit. Manuf. 6 (1) (2019) 31–39.
[41] Q. Shi, et al., Recyclable 3D printing of vitrimer epoxy, Mater. Horiz. 4 (4) (2017) 598–607.
[42] X. Shi, C. Luo, H. Lu, K. Yu, Primary recycling of anhydride-cured engineering epoxy using alcohol solvent, Polym. Eng. Sci. 59 (s2) (2019) E111–E119.
[43] P. Taynton, et al., Repairable woven carbon fiber composites with full recyclability enabled by malleable polyimine networks, Adv. Mater. 28 (15) (2016) 2904–2909.
[44] D. Montarnal, M. Capelot, F. Tournilhac, L. Leibler, Silica-like malleable materials from permanent organic networks, Science 334 (6058) (2011) 965–968.
[45] K. Yu, et al., Reprocessing and recycling of thermosetting polymers based on bond exchange reactions, RSC Adv. 4 (20) (2014) 10108–10117.
[46] K. Yu, et al., Influence of stoichiometry on the glass transition and bond exchange reactions in epoxy thermoset polymers, RSC Adv. 4 (89) (2014) 48682–48690.
[47] K. Yu, et al., Interfacial welding of dynamic covalent network polymers, J. Mech. Phys. Solid. 94 (2016) 1–17.
[48] X. Shi, et al., A multiscale chemomechanics theory for the solvent–assisted recycling of covalent adaptable network polymers, J. Mech. Phys. Solid. (2020) 103918.
[49] X. Shi, et al., Evolution of material properties during the solvent-assisted recycling of thermosetting polymers: to reduce the residual stress and material inhomogeneity, Materials Today Sustainability 19 (2022) 100167.
[50] X. Shi, et al., Influences of material and processing conditions on the depolymerization speed of anhydride-cured epoxy during the solvent-assisted recycling, Polymer 252 (2022) 124964.
[51] G.A. Holzapfel, Nonlinear Solid Mechanics: a Continuum Approach for Engineering, 2000. New York: Wiley, Chichester.
[52] M.C. Boyce, D.M. Parks, A.S. Argon, Computational modeling of large strain plastic-deformation in glassy-polymers, Abstr. Pap. Am. Chem. Soc. 196 (1988) 156–POLY.
[53] K.K. Westbrook, et al., A 3D finite deformation constitutive model for amorphous shape memory polymers: a multi-branch modeling approach for nonequilibrium relaxation processes, Mech. Mater. 43 (12) (2011) 853–869.
[54] M. Rubinstein, R.H. Colby, Polymer Physics, first ed., Oxford University Press, 2003.
[55] V.V. Krongauz, Diffusion in polymers dependence on crosslink density, J. Therm. Anal. Calorim. 102 (2) (2010) 435–445.
[56] S.A. Lima, M. Kamrujjaman, M.S. Islam, Numerical solution of convection-diffusion-reaction equations by a finite element method with error correlation, AIP Adv. 11 (8) (2021).
[57] Z. Gharibi, M. Dehghan, Convergence analysis of weak Galerkin flux-based mixed finite element method for solving singularly perturbed convection-diffusion-reaction problem, Appl. Numer. Math. 163 (2021) 303–316.
[58] R.C. Lin, X. Ye, S.Y. Zhang, P. Zhu, A weak galerkin finite element method for singularly perturbed convection-diffusion-reaction problems, SIAM J. Numer. Anal. 56 (3) (2018) 1482–1497.
[59] G.R. Barrenechea, A.H. Poza, H. Yorston, A stabilised finite element method for the convection-diffusion-reaction equation in mixed form, Comput. Methods Appl. Mech. Eng. 339 (2018) 389–415.
[60] C.M. Hamel, X. Kuang, H.J. Qi, Modeling the dissolution of thermosetting polymers and composites via solvent assisted exchange reactions, Compos. B Eng. (2020) 200.
[61] Y. Mao, et al., A viscoelastic model for hydrothermally activated malleable covalent network polymer and its application in shape memory analysis, J. Mech. Phys. Solid. 127 (2019) 239–265.
[62] C. Luo, C. Chung, K. Yu, A diffusion-reaction computational study to reveal the depolymerization mechanisms of epoxy composites for recycling, Materials Today Sustainability 23 (2023) 100452.